

Mathematical Modelling of Heating and Evaporation of a Spheroidal Droplet

Vladimir Zubkov^{*1}, Gianpietro E. Cossali², Simona Tonini¹, Cyril Crua¹, Sergei S. Sazhin¹

¹School of Computing, Engineering and Mathematics, University of Brighton, Brighton, BN2 4GJ, UK

²Department of Engineering and Applied Sciences, University of Bergamo, Viale Marconi 5, 24044 Dalmine, Italy

*Corresponding author: v.zubkov@brighton.ac.uk

Abstract

Most of the currently used models of droplet heating and evaporation are based on the assumption that droplets are perfect spheres. At the same time the shapes of many observed droplets in engineering applications are far from spherical. We have studied the influence of droplet non-sphericity, approximating droplet shapes using prolate spheroids. The evaporation process of a spheroidal droplet in a gaseous atmosphere has been modelled. The previously developed exact solutions to the heat and mass transfer equations for the gas phase surrounding a spheroidal droplet have been used to perform numerical analysis of spheroidal droplet heating and evaporation. The temperature gradient inside droplets and the changes in their shape during the evaporation process have been taken into account. Our results show that significant changes in evaporation rate can be observed even for uniform droplet surface temperature. However, higher evaporation at the droplet surface regions with higher curvature does not mean that droplet eccentricity tends towards 1 (i.e. the droplet does not become more spherical). Our results demonstrate that temperature of a deformed droplet becomes uniform very quickly and after that the deformation parameter remains almost constant during the process of evaporation.

Introduction

The models of droplet heating and evaporation described so far have been based on the assumption that droplets are perfect spheres [1]. At the same time the shapes of most actually observed droplets in engineering and environmental applications are far from spherical [2, 3]. In most cases the effects of non-sphericity of droplets has been investigated assuming that droplet shapes can be approximated by those of prolate or oblate spheroids.

The heat conduction equation inside a spheroidal body (droplet) was first (to the best of our knowledge) solved analytically more than 135 years ago [4]. This solution, however, turned out to be too complex for most practical applications. In most cases this problem (and the related problem of mass transfer inside the body) has been investigated based on the numerical solutions to heat transfer (and mass diffusion) equations [5, 6].

The problem of heat/mass transfer inside spheroidal bodies, considered in the above-mentioned papers, is complementary to the problem of heat/mass transfer from/to ambient fluid (gas) to/from a spheroidal body, taking into account the relative velocity between gas and the body, in the general case. The latter problem has been considered in numerous papers based on the numerical solutions to the momentum and heat transfer equations in the ambient fluid (gas) in the ellipsoidal coordinate system. The analysis of [7, 8, 9, 12, 13] was based on the assumption that the body surface temperature was fixed. Juncu [14] took into account changes in body temperature with time, while assuming that there is no temperature gradient inside the body (the thermal conductivity of the body was assumed infinitely high).

These approaches are equally applicable to solid bodies and droplets. In the case of droplets, however, apart from heating, the evaporation processes should also be taken into account in the general case. Grow [15] was perhaps the first to solve the problem of heat and mass transfer in the vicinity of spheroidal particles assuming that their relative velocities are equal to zero, although she considered coal chars rather than droplets. One of the main limitations of that paper is that both mass and heat transfer equations were presented in the form of Laplace equations, which implies that the effects of the Stefan flow from the surface of the particles were ignored. The latter effects were taken into account in the exact solutions to the mass and heat transfer equations in the gas phase around a spheroidal droplet in the model suggested in [16]. In that paper it was assumed that the temperatures at all points at the surface of the droplet are the same and constant, and the droplet's shape remains the same. A combined problem of spheroidal droplet heating and evaporation, similar to the one studied in [16], was considered in [17]. As in [16], the authors of [17] based their analysis on the solution to the species conservation equation in the gas phase and assumed that the thermal conductivity of droplets is infinitely large. In contrast to [16], the authors of [17] took into account the relative velocities of droplets, assuming that the dependence of the Nusselt and Sherwood numbers on the Reynolds and Prandtl numbers are the same as those for spherical droplets. Also, they took into account the time dependence of droplet temperatures and sizes, although their analysis was focused on oblate droplets only.

As follows from a brief overview of the models described above, a model of heating and evaporation of spheroidal droplets is far from being developed. We believe, however, that the results presented in [16] could be considered as a starting point for constructing this model at least for the cases of spheroids with the shapes not too different from those of spheres (slightly deformed spheres). The main ideas of the model described in [16] and its possible generalisations are summarised in the next section.

Model description

The model that will be developed here starts with the analysis reported in [16], which was focused on exact solutions to the mass and heat transfer equations in the gas phase around a spheroidal droplet, assuming a uniform (Dirichlet) boundary condition along the drop surface. The model will be extended to account for non-uniform conditions on the droplet surface, assuming that the droplet surface does not deviate greatly from the spherical.

A mathematical model of the gas phase around a spheroidal droplet

The droplet was assumed to be mono-component and the following steady-state equation for the vapour mass fraction ($Y_v = \rho_v / \rho_{tot}$) was solved in the gas phase:

$$\nabla (\rho_{tot} \mathbf{U} Y_v - \rho_{tot} D_v \nabla Y_v) = 0, \quad (1)$$

where $\rho_{tot} = \rho_v + \rho_a$ is the density of the mixture of vapour (with density ρ_v) and ambient air (with density ρ_a), \mathbf{U} is the Stefan velocity of the mixture of vapour and air, D_v is the diffusion coefficient of vapour in air.

Eq. (1) was solved in ellipsoidal coordinates ξ, u, φ defined as:

$$\left. \begin{aligned} x &= a\Phi_-(\xi) \sin(u) \cos(\varphi) \\ y &= a\Phi_-(\xi) \sin(u) \sin(\varphi) \\ z &= a\Phi_+(\xi) \cos(u) \end{aligned} \right\}$$

where

$$\Phi_{\pm}(\xi) = \frac{e^{\xi} \pm s(\varepsilon)e^{\varepsilon\xi}}{2}, \quad s(\varepsilon) = \text{sign}(\varepsilon - 1), \quad \varepsilon = a_z/a_r, \quad (2)$$

$2a_z$ and $2a_r$ are the sizes of the spheroid along and perpendicular to the z -axis, respectively ($\varepsilon > 1$ and $s = 1$ for prolate spheroids, $\varepsilon < 1$ and $s = -1$ for oblate spheroids)*. It can be shown that the coordinate u is linked with $\theta = \arctan \left[\sqrt{x^2 + y^2} / z \right]$ by the following relation: $\tan u = \varepsilon \tan \theta$, valid for both prolate and oblate spheroids.

In this coordinate system the spheroidal surface is defined by the equation $\xi = \xi_0 = \text{const}$ and

$$\xi_0 = \ln \sqrt{\frac{\varepsilon^s + 1}{\varepsilon^s - 1}}; \quad a = R_0 \frac{|1 - \varepsilon^2|^{1/2}}{\varepsilon^{1/3}}, \quad (3)$$

where R_0 is the radius of a sphere which has the same volume as the spheroid.

The authors of [16] solved Eq. (1) assuming that the values of Y_v and all other scalar properties are the same along the whole surface of the droplet (Dirichlet conditions) and equal to $Y_v = Y_{v,s}$, and Stefan velocity and diffusive fluxes are perpendicular to the droplet surface ($\mathbf{U} = (U_{\xi}, 0, 0)$). These assumptions allowed the authors to simplify Eq. (1) to:

$$\rho_{tot} U_{\xi} \frac{dY_v}{d\xi} = \frac{D_v}{aS^2} \frac{d}{d\xi} \left[\rho_{tot} \Phi_-(\xi) \frac{dY_v}{d\xi} \right], \quad (4)$$

where

$$S^2 \equiv S^2(\xi, u) = \Phi_-(\xi) [\Phi_-^2(\xi) \cos^2 u + \Phi_+^2(\xi) \sin^2 u]^{1/2}. \quad (5)$$

Note that Eq. (4) is different from the one on which the analysis of [17] was based (see their Eq. (10)). The latter equation is the Laplace-type equation which is valid only in the case when the effect of the Stefan flow is ignored.

Eq. (4) was solved assuming that, at large distances from the droplet $Y_v = Y_{v\infty} = \text{const}$ and the validity of the condition $\rho_{tot} = \rho_v + \rho_a = \text{const}$ (see [1]). The local vapour flux ($n_{v,s}$) and the evaporation rate (\dot{m}_{ev}) were found as [16]:

$$n_{v,s} = \frac{\varepsilon^{2/3}}{|1 - \varepsilon^2| S^2(\xi, u)} \frac{\dot{m}_{ev}}{4\pi R_0^2}$$

$$\dot{m}_{ev} = 4\pi R_0 \rho D_v \Gamma(\varepsilon) \ln \frac{1 - Y_{v\infty}^{(v)}}{1 - Y_{v,s}^{(v)}} \quad (6)$$

*Note that in [12, 13] prolate and oblate spheroids were defined as those with $\varepsilon < 1$ and $\varepsilon > 1$ respectively; it seems that the same definition is used in Fig. 1 of [9].

where

$$\Gamma(\varepsilon) = \frac{|1 - \varepsilon^2|^{1/2}}{\varepsilon^{1/3}} \begin{cases} \frac{1}{\pi - 2 \arctan\left(\sqrt{\frac{1+\varepsilon}{1-\varepsilon}}\right)} & \text{oblate} \\ \frac{1}{\ln\left(\sqrt{\frac{1+\varepsilon}{\varepsilon-1}}+1\right) - \ln\left(\sqrt{\frac{1+\varepsilon}{\varepsilon-1}}-1\right)} & \text{prolate} \end{cases} \quad (7)$$

As mentioned earlier, in the original paper [16] it was assumed that $Y_{vs} = \text{const}$. In the general case these formulae could be applied to the case when $Y_{vs} = Y_{vs}(u)$ provided that the spheroid can be considered as a slightly deformed sphere (ε is close to 1).

The assumption $\rho_{\text{tot}} = \rho_v + \rho_a = \text{const}$ was relaxed in [18]. The generalisation of the approach suggested in [18] to the case of spheroidal droplets has not been considered to the best of our knowledge.

Under the above-mentioned assumptions, the energy conservation equation can be presented as:

$$\rho_{\text{tot}} \mathbf{U} c_p \nabla T = k_g \nabla^2 T, \quad (8)$$

where c_p is the specific heat capacity at constant pressure and k_g is the thermal conductivity of the gas (a mixture of fuel vapour and air in the general case). This equation can be solved for spheroidal coordinates, for uniform temperature distribution along the droplet surface, assuming that the temperature at a large distance from the droplet is equal to $T_\infty = \text{const}$. The final equation for the temperature distribution was obtained in the form [16] :

$$T = \frac{T_\infty - T_s}{1 - \eta} \left[\eta^{\zeta(\xi, \varepsilon)} - \eta \right] + T_s, \quad (9)$$

where

$$\eta = \exp \left[-\frac{1}{\text{Le}} \ln \frac{1 - Y_{v\infty}}{1 - Y_{vs}} \right], \quad (10)$$

$$\zeta(\xi, \varepsilon) = \begin{cases} \frac{\pi - 2 \arctan(e^\xi)}{\pi - 2 \arctan\left(\sqrt{\frac{1+\varepsilon}{1-\varepsilon}}\right)} & \text{oblate} \\ \frac{\ln(e^\xi + 1) - \ln(e^\xi - 1)}{\ln(\varepsilon + \sqrt{\varepsilon^2 - 1})} & \text{prolate} \end{cases}$$

$\text{Le} = k_g / (\rho_{\text{tot}} c_p D_v)$ is the Lewis number.

Extension of the model to non-uniform boundary conditions

In the original paper [16], Eq. (4) was derived under the assumption that Y_v is the same along the whole surface of the droplet. This assumption implied that the tangential component of the temperature gradient along the surface of the droplet is nil, which follows from another assumption made by [16] that droplet thermal conductivity is infinitely large.

Considering heat transfer from the evaporating droplet, essentially the same analysis as presented above can be repeated, using the weaker assumption that the gradients of temperature in the directions perpendicular to the droplet surface are much larger compared with those along this surface. This assumption is expected to be valid in the case when the sphericity of the droplet ε is reasonably close to 1. In this case η becomes a function of u in the general case (recall that $Y_{vs} = Y_{vs}(T_s)$).

Expression (9) allows us to find the local convective heat transfer coefficient h based on the following formula:

$$h = -\frac{\left. -k_g \nabla T \right|_{\xi=\xi_0}}{|T_\infty - T_s|}. \quad (11)$$

Although the value of h was not explicitly calculated in [16], this calculation follows in a straightforward way from the previous analysis by these authors:

$$h = \frac{k_g \eta}{R_0 (1 - \eta)} \begin{cases} \frac{\varepsilon^{1/3}}{\left[\pi - 2 \arctan\left(\sqrt{\frac{1+\varepsilon}{1-\varepsilon}}\right) \right] \sqrt{\left(\frac{1}{1-\varepsilon^2} - \sin^2 u\right)}} & \text{oblate} \\ \frac{\varepsilon^{1/3}}{\left[\ln(\varepsilon + \sqrt{\varepsilon^2 - 1}) \right] \sqrt{\left(\frac{1}{\varepsilon^2 - 1} - \sin^2 u\right)}} & \text{prolate} \end{cases} \quad (12)$$

where η is defined by Expression (10).

Perhaps the most important limitation of the model summarised above is that it does not take into account the changes in the shape of the droplets during the evaporation process. A simplified model, taking into account these changes and predicting the time evolution of redistribution of the temperature inside droplets is described in the next section.

A model for temperature distribution and shape evolution of an evaporating droplet

The transient heating of an evaporating droplet is governed by the following equation in the liquid phase:

$$\rho_f c_f \frac{\partial T}{\partial t} - \nabla(k_f \nabla T) = 0, \quad (13)$$

where k_f is thermal conductivity, ρ_f is density and c_f is the specific heat capacity of liquid fuel. The analytical solution for the gas phase around a spheroidal droplet, presented in [16] and discussed above, was used for the boundary condition at the droplet surface:

$$-\mathbf{n}(-k_f \nabla T) = q + h(T_\infty - T) \quad \text{at} \quad \xi = \xi_0, \quad (14)$$

where \mathbf{n} is the unit normal vector to the droplet surface, the convective heat transfer coefficient h is defined by (12) and q is the heat flux due to evaporation that will be specified later.

We take into account the decrease in the droplet size due to evaporation but not the effect of thermal swelling. The shape of the droplet is recalculated at each time step of numerical simulations assuming that the droplet remains spheroidal and the sizes of the spheroidal droplet along and perpendicular to the z -axis are governed by following ordinary differential equations and initial conditions:

$$a'_r(t) = -\frac{1}{\rho_f} \frac{dm}{dA} \Big|_{u=\pi/2}, \quad a'_z(t) = -\frac{1}{\rho_f} \frac{dm}{dA} \Big|_{u=0}, \quad (15)$$

$$a_r(0) = a_{r0}, \quad a_z(0) = a_{z0},$$

where evaporation mass flux $\frac{dm}{dA}$ varies along the droplet surface and is defined by Eq. (6). To relate temperature, T , and the vapour mass fraction, $Y_v = \rho_v/\rho_{\text{tot}}$, at the droplet surface and far from the droplet we use the ideal gas law

$$\rho_{vs} = \frac{M_v P_s}{R_u T_s}, \quad \rho_{v\infty} = 0, \quad (16)$$

$$\rho_{as} = \frac{M_a (P - P_s)}{R_u T_s}, \quad \rho_{a\infty} = \frac{M_a P}{R_u T_\infty}, \quad (17)$$

where P is the ambient gas pressure and P_s is the saturated vapour pressure, R_u is the universal gas constant, M_v and M_a are molar masses of the vapour and the ambient air, respectively. Following Abramzon and Sazhin ([19]), we define the saturated vapour pressure, the diffusion coefficient of vapour in air, thermal conductivity of liquid fuel, the specific heat capacity of liquid fuel, and the heat flux due to evaporation for n-dodecane $C_{12}H_{26}$ as

$$P_s = \exp(8.1948 - 7.8099(300/T_s) - 9.0098(300/T_s)^2) \quad (\text{bar}), \quad (18)$$

$$D_v = 5.27 \cdot 10^{-6} (T/300)^{1.583} P^{-1} (\text{m}^2/\text{s}) (P \text{ in bar}), \quad (19)$$

$$k_f = 0.1405 - 0.00022(T - 300) \quad (\text{W/m K}), \quad (20)$$

$$c_f = 2.18 + 0.0041(T - 300) \quad (\text{kJ/kg K}), \quad (21)$$

$$q = 37.44 \cdot 10^3 (T_{cr} - T)^{0.38} \rho_f v_n, \quad (22)$$

where $T_{cr} = 659$ (K) is the critical temperature, v_n is the normal velocity of the recession of the evaporating surface of the droplet,

$$v_n = v_r n_r + v_z n_z, \quad (23)$$

$$v_r = -r(r^2 a'_r/a_r^3 + z^2 a'_z/a_z^3), \quad v_z = z(r^2 a'_r/a_r^3 + z^2 a'_z/a_z^3), \quad (24)$$

$$n_r = -r/a_r^2 \sqrt{r^2/a_r^4 + z^2/a_z^4}, \quad n_z = -z/a_z^2 \sqrt{r^2/a_r^4 + z^2/a_z^4}. \quad (25)$$

Assuming that the contribution of fuel vapour to the thermal conductivity and heat capacity of the mixture of vapour and air can be ignored, we can write [10, 11]

$$k_g = 0.0036 + 0.0252(T/300) - 0.00189(T/300)^2 \quad (\text{W/m K}), \quad (26)$$

$$c_p = 0.963 + 0.0514(T/300) \quad (\text{kJ/kg K}). \quad (27)$$

Our model is based on the assumption that at each stage of heating and evaporation, the droplet shape can be approximated by that of a spheroid but with time dependent a_r and a_z . The initial distribution of the temperature is assumed to be uniform inside the droplet, $T = T_d$, and the temperature in the ambient gas, T_∞ , is assumed to be constant.

The parameters used in the model and numerical methods used in the analysis are described in the next section.

Parameters of the model and numerical methods

We model a droplet of n-dodecane $C_{12}H_{26}$ surrounded by air. The parameters of the model are presented in Table 1.

| Parameter | Value | Notes |
|-----------------|------------------------|----------------------------------|
| ε_0 | 1.5 | initial droplet deformation |
| R_0 | 10^{-5} m | initial effective droplet radius |
| T_d | 300 K | initial droplet temperature |
| T_∞ | 700 K | ambient gas temperature |
| P | 30 bar | ambient gas pressure |
| R_u | 8.3154 J/(K mol) | universal gas constant |
| M_v | $170.33 \cdot 10^{-3}$ | molar mass of vapour |
| M_a | $28.97 \cdot 10^{-3}$ | molar mass of ambient air |
| T_{cr} | 659 K | critical temperature |

Equations (13)-(15) were solved numerically. These were integrated using the finite-element-based PDE modules of COMSOL Multiphysics including Moving Mesh (ALE). We made sure that the solutions remained unaffected by the mesh size and time step below certain minimal values.

Results

In this section, we consider numerical solutions to Equations (13)-(15), describing heating and evaporation processes in a liquid spheroidal droplet surrounded by air. Functionality testing of the model was carried out to ensure that the solution for spherical droplets agrees with the predictions of the model in the limiting case when spheroidal droplets become spherical.

In Fig. 1 we demonstrate the temperature profile along a vertical cross section of a prolate evaporating droplet at four time instants. Droplet initial deformation parameter $\varepsilon_0 = 1.5$ and the initial effective radius $R_0 = 10^{-5}$ m (the effective radius of a deformed droplet is the radius of a spherical droplet of the same volume). As follows from Fig. 1B, initially, the temperatures inside the droplet and at its surface vary over time and reach the highest value at the droplet tips where the surface curvature is the highest. However, very rapidly the temperature profile becomes uniform and does not change over time (see Figs. 1C and 1D). This constant temperature corresponds to the case when the right-hand side of Equation (14) is zero: $T_s = q/h + T_\infty$.

Fig. 2A shows a schematic of a prolate droplet with an initial deformation parameter $\varepsilon_0 = 1.5$; a_r and a_z are halves of the radial and axial droplet semi-axes. Fig. 2D shows that evaporation at the droplet surface regions with higher curvature (e.g. point B in Fig. 2A) is higher than at point A. However, higher evaporation does not necessarily mean that droplet eccentricity will move towards 1. This suggests that the evaporation of a prolate droplet does not cause it to become more spherical. What follows is our possible explanation of this phenomenon. In Fig. 2C, we demonstrate that local temperatures at point A, T_A , and point B, T_B , of the deformed droplet surface can vary noticeably. As in the case shown in Fig. 1, Fig. 2C confirms that the temperature profile becomes uniform rather rapidly. Using (15) for constant temperature along the droplet surface, we obtain, $a'_z/a'_r = \varepsilon$. Thus, once the temperature along the droplet surface becomes uniform, the ratio $a'_z/a'_r = \varepsilon$, which, in turn, keeps the ratio $\varepsilon = a_z/a_r$ constant. Indeed, at the initial stage of the simulation, ratio ε in Fig. 2B slightly decreases. During this period, the temperature difference between points A and B is noticeable. At $t = 10^{-3}$ s, temperature becomes uniform and $\varepsilon = 1.49$ no longer changes with time.

Fig. 3 shows how the effective radius of a droplet changes with time due to evaporation. It demonstrates that a prolate droplet, with an initial deformation parameter $\varepsilon_0 = 1.5$ and initial effective radius $R_0 = 10^{-5}$ m, evaporates slightly faster (1.4%) than a spherical droplet of the same initial volume. This observation can be partially explained by the bigger surface area of the deformed droplet compared with the spherical one. The bigger surface leads to a higher evaporation mass flux for the entire droplet.

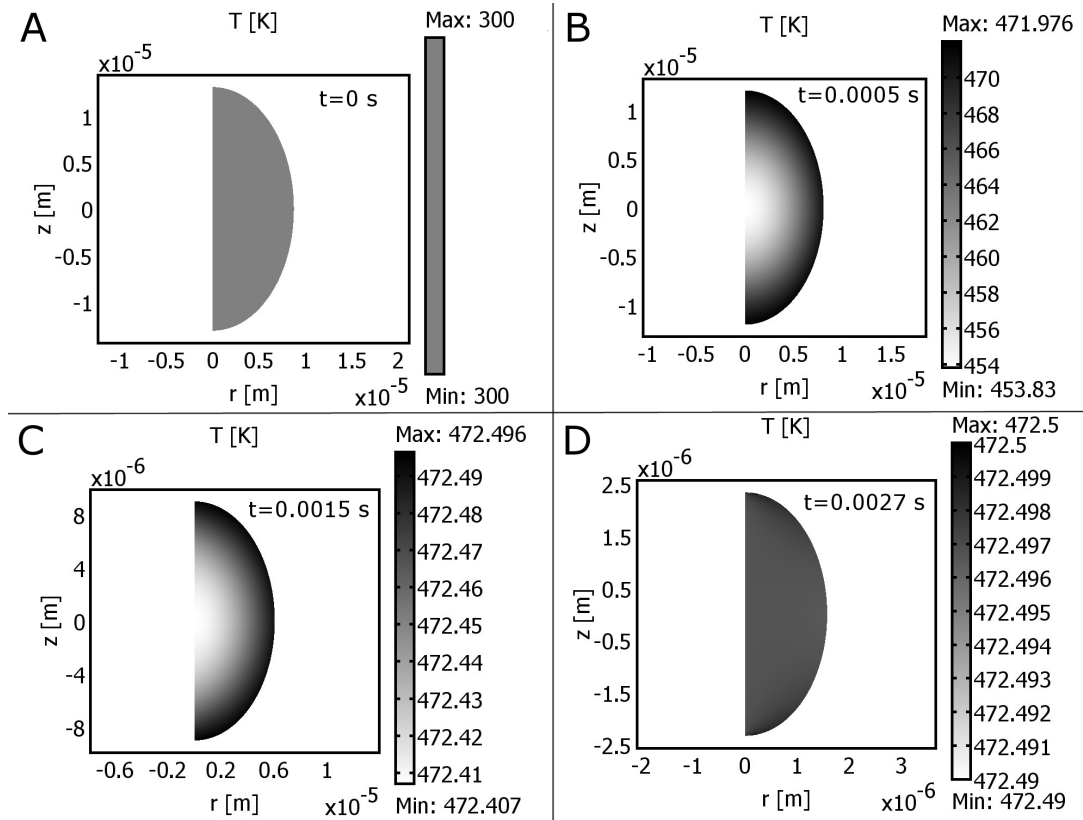


Figure 1. Temperature profiles along a vertical cross section of a prolate droplet at different times: A) $t = 0$ s, B) $t = 0.0005$ s, C) $t = 0.0015$ s, D) $t = 0.0027$ s. Drop initial temperature, $T_d = 300$ K; ambient gas temperature, $T_\infty = 700$ K; gas pressure, $P = 30$ bar.

Conclusions

We considered a mathematical model for heating and evaporation processes of a liquid spheroidal droplet. Assuming axial symmetry of the droplet (relative to the z -axis), the 3D problem was reduced to a 2D problem. We studied how non-sphericity of a droplet affects its evaporation and geometry. Our results show that local temperatures can vary noticeably along the droplet surface only during the initial stage of the process and significant changes in evaporation rate can be observed even for uniform surface temperature. However, higher evaporation at the droplet surface regions with higher curvature does not mean that the droplet eccentricity tends towards 11 (i.e. the droplet does not become more spherical). Our results demonstrate that the temperature of a deformed droplet (deformation parameter is 1.5) becomes uniform very quickly and the deformation parameter $\varepsilon = a_z/a_r$ becomes almost constant during the process of evaporation.

Acknowledgements

The authors are grateful to EPSRC (UK) (Project EP/K020528/1) for the financial support of this project.

Nomenclature

| | |
|-------|--|
| a_r | size of the spheroid perpendicular to the z -axis [m] |
| a_z | size of the spheroid along the z -axis [m] |
| c_f | specific heat capacity of liquid fuel [J/kgK] |
| c_p | specific heat capacity of gas [J/kgK] |
| D_v | diffusion coefficient of vapour in air [m^2/s] |
| h | convective heat transfer coefficient [$\text{W}/(\text{m}^2\text{K})$] |
| k_g | thermal conductivity of gas [$\text{W}/(\text{mK})$] |
| k_f | thermal conductivity of liquid fuel [$\text{W}/(\text{mK})$] |
| Le | Lewis number [-] |
| M_a | molar mass of ambient air [kg/mol] |

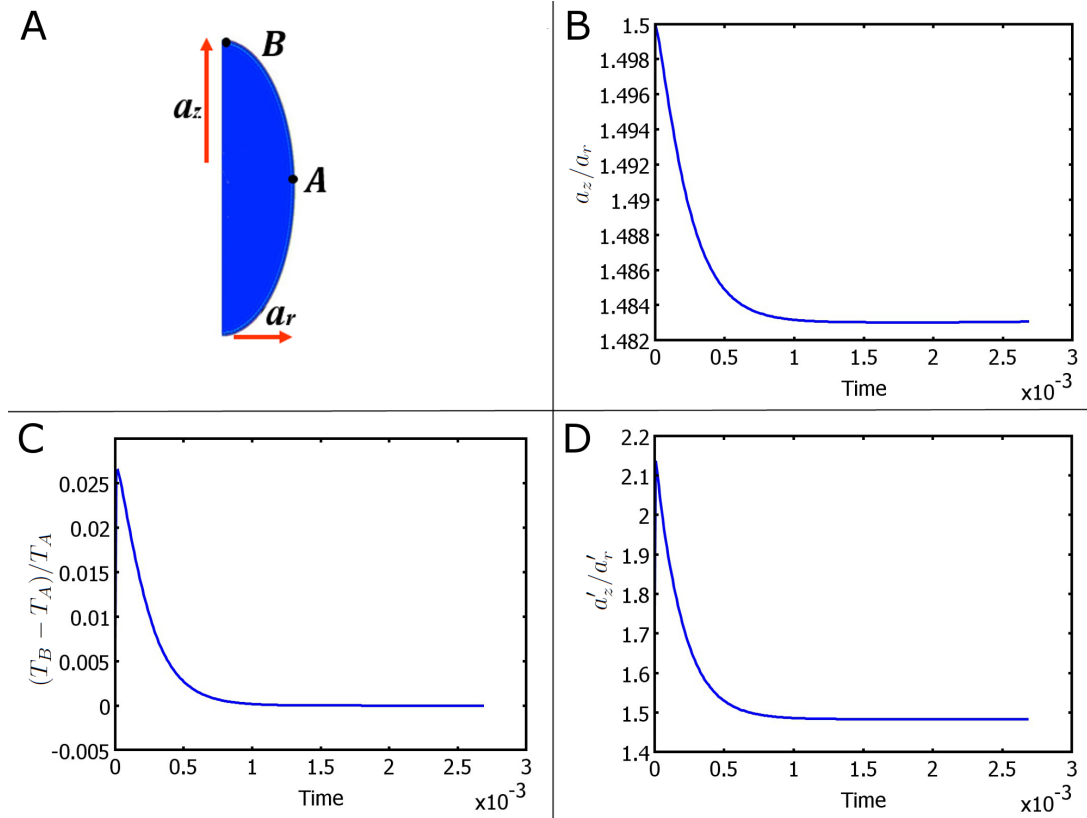


Figure 2. (A) A schematic of a prolate droplet with an initial deformation parameter $\varepsilon_0 = 1.5$; a_r and a_z are halves of the radial and axial droplet semi-axes; (B) ratio $\varepsilon = a_z/a_r$ versus time (s); (C) Relative temperature difference at points A and B of a droplet versus time (s); T_A and T_B are the surface temperatures at points A and B, respectively; (D) ratio a'_z/a'_r vs time. Droplet initial temperature, $T_d = 300$ K; ambient gas temperature, $T_\infty = 700$ K; gas pressure, $P = 30$ bar.

| | |
|-----------------|---|
| \dot{m}_{ev} | mass evaporation rate [kg/s] |
| M_v | molar mass of vapour [kg/mol] |
| $n_{v,s}$ | local vapour flux [kg/(m ² s)] |
| P | ambient gas pressure [bar] |
| P_s | saturated vapour pressure [bar] |
| q | heat flux due to evaporation [W/(m ²)] |
| R | effective droplet radius [m] |
| R_u | universal gas constant [J/(K mol)] |
| R_0 | initial effective droplet radius [m] |
| S | function defined by Eq. (5) |
| t | time [s] |
| T | temperature [K] |
| T_{cr} | critical temperature [K] |
| T_d | initial droplet temperature [K] |
| T_∞ | ambient gas temperature [K] |
| \mathbf{U} | Stefan velocity of the mixture of vapour and air [m/s] |
| v_n | normal velocity of the evaporating surface of the droplet [m/s] |
| x,y,z | Cartesian coordinates [-] |
| Y_v | vapour mass fraction [-] |
| α | species [-] |
| ε | droplet deformation parameter [-] |
| ε_0 | initial droplet deformation parameter [-] |
| Γ | evaporation enhancement defined by Eq. (7) |
| η | function defined by Eq. (10) |
| Φ | function defined by Eq. (2) |
| ρ_a | air density [kg/m ³] |
| ρ_f | liquid fuel density [kg/m ³] |

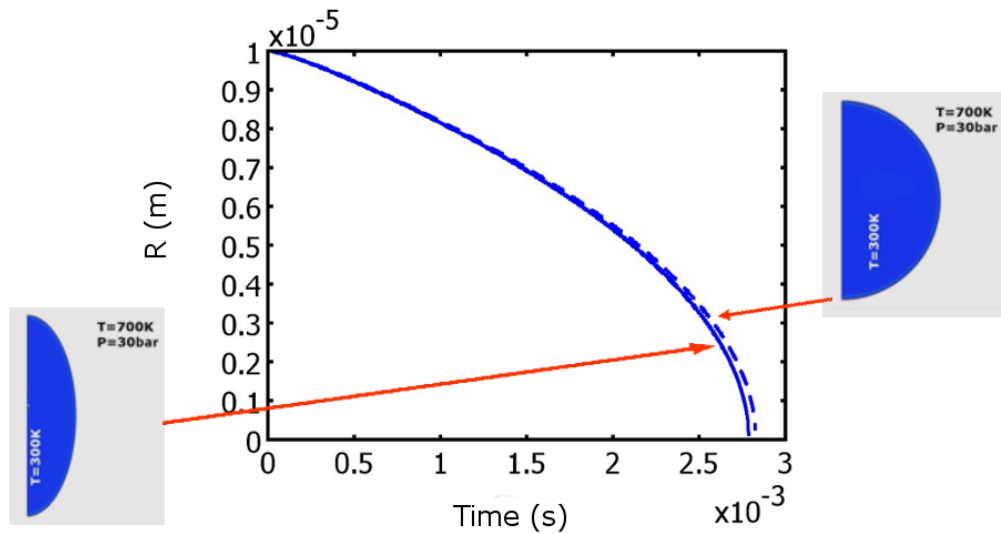


Figure 3. Effective radii of prolate (solid) and spherical (dashed) droplets versus time during heating and evaporation processes. Droplet initial temperature, $T_d = 300$ K; surrounding gas temperature, $T_\infty = 700$ K; gas pressure, $P = 30$ bar.

ρ_v vapour density [kg/m^3]
 ρ_{tot} density of the mixture of vapour and ambient air [kg/m^3]
 ξ, u, φ ellipsoidal coordinates [-]

References

- [1] Sazhin, S., 2014, "Droplets and Sprays". Springer.
- [2] Michaelides, E., 2006, "Particles, Bubbles and Drops". World Scientific.
- [3] Crua, C., Heikal, M. R. and Gold, M. R., 2015, Fuel, 157, pp. 140-150.
- [4] Niven, C., 1880, Philosophical Transactions of the Royal Society London, 171, pp. 117-151.
- [5] Jog, M. A., H., 1997, International Journal of Heat and Fluid Flow, 18, pp. 411-418.
- [6] Lima, D., Farias, S. and Lima, G., 2004, Brazilian Journal of Chemical Engineering, 21, pp. 667-680.
- [7] Alassar, R., 2005, ASME Journal of Heat Transfer, 127, pp. 1062-1070.
- [8] Richter, A., Nikrityuk, P., 2012, International Journal of Heat and Mass Transfer, 55, pp. 1343-1354.
- [9] Kishore, N., Gu, S., 2011, International Journal of Heat and Mass Transfer, 55, pp. 2595-2601.
- [10] Sazhin, S. S., Al Qubeissi, M., Kolodnytska, R., Elwardany, A. E., Nasiri, R. and Heikal, M. R., 2014, Fuel, 115, pp. 559-572.
- [11] Incropera, F. P., Dewitt, D. P., 2002, "Fundamentals of heat and mass transfer". Jon Wiley and Sons.
- [12] Sreenivasulu, B., Srinivas, B. and Ramesh, K., 2014, International Journal of Heat and Mass Transfer, 70, pp. 71-80.
- [13] Sreenivasulu, B., Srinivas, B., 2015, International Journal of Thermal Sciences, 87, pp. 1-18.
- [14] Juncu, G., 2010, International Journal of Heat and Mass Transfer, 53, pp. 3483-3494.
- [15] Grow, D., 1990, Combustion and Flame, 80, pp. 209-213.
- [16] Tonini, S., Cossali, G., 2013, International Journal of Heat and Mass Transfer, 60, pp. 236-240.
- [17] Li, J., Zhang, J., 2014, Physics Letters A, 378 (47), pp. 3537-3543.

[18] Tonini, S., Cossali, G., 2012, *International Journal of Thermal Sciences*, 57, pp. 45-53.

[19] Abramzon, B., Sazhin, S., 2006, *Fuel*, 85 (1), pp. 32-46.